Structural Analysis of Botulinum Neurotoxin Type E Catalytic Domain and Its Mutant Glu212→Gln Reveals the Pivotal Role of the Glu212 Carboxylate in the Catalytic Pathway[†,‡]

Rakhi Agarwal,[#] Subramaniam Eswaramoorthy,[#] Desigan Kumaran,[#] Thomas Binz,[§] and Subramanyam Swaminathan*[,#]

Biology Department, Brookhaven National Laboratory, Upton, New York 11973, and Department of Biochemistry, Medizinische Hochschule Hannover, Hannover, Germany

Received December 18, 2003; Revised Manuscript Received March 9, 2004

ABSTRACT: The seven serotypes of botulinum neurotoxins (A−G) produced by *Clostridium botulinum* share significant sequence homology and structural similarity. The functions of their individual domains and the modes of action are also similar. However, the substrate specificity and the peptide bond cleavage selectivity of their catalytic domains are different. The reason for this unique specificity of botulinum neurotoxins is still baffling. If an inhibitor leading to a therapeutic drug common to all serotypes is to be developed, it is essential to understand the differences in their three-dimensional structures that empower them with this unique characteristic. Accordingly, high-resolution structures of all serotypes are required, and toward achieving this goal the crystal structure of the catalytic domain of *C. botulinum* neurotoxin type E has been determined to 2.1 Å resolution. The crystal structure of the inactive mutant Glu212→Gln of this protein has also been determined. While the overall conformation is unaltered in the active site, the position of the nucleophilic water changes in the mutant, thereby causing it to lose its ability to activate the catalytic reaction. The structure explains the importance of the nucleophilic water and the charge on Glu212. The structural differences responsible for the loss of activity of the mutant provide a common model for the catalytic pathway of *Clostridium* neurotoxins since Glu212 is conserved and has a similar role in all serotypes. This or a more nonconservative mutant (e.g., Glu212→Ala) could provide a novel, genetically modified protein vaccine for botulinum.

Clostridium botulinum secretes seven serotypes of botulinum neurotoxins (BoNT,[1] A−G) that are produced as single inactive polypeptide chains of 150 kDa and cleaved into active dichains of heavy (HC, 100 kDa) and light (LC, 50 kDa) chains, linked by a disulfide bond, by endogenous or exogenous proteases. The HC mediates binding to nerve cells and translocation of the catalytical LC into the cytosol following receptor-mediated endocytosis.

Although they all share sequence and possibly structural similarity, each BoNT has exclusive substrate specificity and scissile bond selectivity (*1*). BoNT/A, /C, and /E cleave the synaptosomal-associated 25-kDa protein (SNAP-25) at different peptide bonds (*2*−*4*), while BoNT/B, /D, /F, and /G cleave the vesicle-associated membrane protein (VAMP), also known as synaptobrevin (*5*), but again each cuts at a different peptide bond. BoNT/C may be unique since it cleaves both SNAP-25 and syntaxin (*1*). The BoNTs are typical zinc metalloproteases which have a unique conserved zinc binding motif (HExxH + E) in the catalytic domain. The Zn coordinated by two histidines, a glutamate and a water molecule, plays an important role in the catalytic activity.

Even though experimental vaccines are available, no therapeutic treatments are on hand to date. To develop a successful vaccine/inhibitor/antitoxin for the toxins, an understanding of the molecular mechanism, especially catalysis by catalytic domain, is a prerequisite. This will help in rational structure-based drug design in the treatment of botulism.

A large body of information on chemical, biological, and pathological aspects of *Clostridium* neurotoxins is available now, but structural information for the holotoxin is available only for BoNT/A at 3.3 Å (*6*) and BoNT/B at 1.8 Å (*7*). Three-dimensional structures are also available for BoNT/A-LC (unpublished work), BoNT/B-LC (*8*), and the C-fragment of tetanus toxin (*9*, *10*). But this is the first structural report for any of the domains of BoNT/E. The crystal structures of BoNT/E-LC and its mutant Glu212Gln are reported here. Comparison of the structures of BoNT/A, BoNT/B, and BoNT/E LCs would provide a basis for

[†] This research has been supported by the U.S. Army Medical Research Acquisition Activity (Award No. DAMD17-02-2-0011) under DOE Prime Contract No. DE-AC02-98CH10886 with Brookhaven National Laboratory.

[‡] The coordinates for the wild-type (1T3A) and mutant (1T3C) structures are deposited with the Protein Data Bank.

* To whom correspondence should be addressed. E-mail: swami@bnl.gov. Telephone: (631) 344-3187. Fax: (631) 344-3407.

[#] Brookhaven National Laboratory.

[§] Medizinische Hochschule Hannover.

[1] Abbreviations used: BoNT, botulinum neurotoxin; HC, heavy chain; LC, light chain; VAMP, vesicle-associated membrane protein; SNAP-25, synaptosomal-associated 25-kDa protein; DTT, dithiothreitol; HEPES, (*N*-[2-hydroxyethyl]piperazine-*N*′-[2-ethanesulfonic acid]); SAD, single-wavelength anomalous dispersion; GST, glutathione-*S*-transferase.

10.1021/bi036278w CCC: $27.50
Published on Web 05/08/2004

understanding the differences in their specificity and selectivity and information for designing a common inhibitor for all three or any of the serotypes. The difference in structure and function of wild-type and mutant (Glu212Gln) of BoNT/E presents a model for the catalytic pathway of the toxin.

EXPERIMENTAL PROCEDURES

Plasmid Construction, Site-Directed Mutagenesis, and Expression and Purification of BoNT/E-LC Protein. The pET-9c vector encoding the full length of BoNT/E-LC has been constructed as described earlier (*11*). This construct (LC-pET9c) has been expressed in BL21 (DE3) cells, and a high level of expression (>30 mg/L of culture) has been achieved. A full description of expression and purification procedures is given by Agarwal et al. (*11*).

The 46mer complementary PCR primers (Invitrogen) were designed to abolish a restriction site by a silent mutation near the site of target mis-sense mutation. The restriction site for *Nsi*I was abolished (A′TGCAT) with the aim to achieve an easy and fast identification of the probable clones containing the mutation. The mutation site was in the middle region of the primers: forward primer 5′CCT GCT CTT ACA TTA *ATG CA*C **C**AA TTA ATA CAT TCA TTA CAT GGA C 3′ and reverse primer 5′GTC CAT GTA ATG AAT GTA TTA ATT **G***GT GCA TTA* ATG TAA GAG CAG G 3′. The underlined 21st and 22nd bases of the forward primer from the 5′ end represent the silent mutation (T→C) to abolish the site for *Nsi*I restriction enzyme and the site of mutation GAA → CAA (E→Q), respectively. The corresponding base changes were also made in the complementary reverse primer. The Quick-Change site-directed mutagenesis kit (Stratagene, La Jolla, CA) was used for the mutagenesis according to the manufacturer's manual. Mutated plasmids were identified by performing *Nsi*I restriction digest through the loss of one *Nsi*I cleavage site. The entire region encoding the mutated LC was sequenced in both strands by Big Dye terminator cycle sequencing (Applied Biosystems) and showed the expected mutation.

The plasmid DNA was transfected into *Escherichia coli* BL21 (DE3) bacteria for the expression of the protein. The growth conditions of the culture for expression and purification of protein used were identical to those described for the wild-type protein (*11*). A similar very high-level expression of protein has been obtained (>15 mg/500 mL of culture). This protein was also found to be very stable and soluble.

Enzymatic Activity of Wild-Type and Mutant Proteins. The proteolytic activity of wild-type and mutant BoNT/E-LC has been assayed in vitro on its substrate SNAP-25(1−206aa). The SNAP-25 had an N-terminal GST tag. The assay was performed in a final volume of 20 μL [20 mM HEPES, pH 7.4, 2 mM DTT, 10 μM $Zn(CH_3COO)_2$] containing a 5 nM concentration of LC and a 5 μM concentration of SNAP-25. However, the mutant protein concentration in reaction mixture was varied from 5 to 50 nM. Cleavage of GST-SNAP-25 by the LC was determined by incubating the samples at 37 °C for 60 min. The reactions were stopped by adding 10 μL of 3× concentrated SDS−PAGE sample buffer which contained sufficient EDTA to chelate the Zn cofactor. The extent of cleavage was then evaluated following electrophoresis on 4−20% Tris−glycine SDS−PAGE gels by the appearance and intensity of a new band at ~47 kDa due to the cleavage of the GST-SNAP-25 between aa180 and 181.

Crystallization and Data Collection. The crystallization screening was carried out by the sitting drop vapor diffusion method using Hampton Research crystallization screens as described previously (*11*). Crystals of both wild-type and mutant proteins were obtained under several conditions using ammonium sulfate and/or PEG at various pH values, ranging from 4.6 to 8.5, at room temperature. Diffraction-quality crystals were obtained at room temperature for both wild-type and mutant proteins using 0.5 M ammonium sulfate, 1.0 M Li_2SO_4, and 0.1 M sodium citrate trihydrate at pH 5.6 as precipitant, and crystals grew to their full size in 2−6 days. Crystals belong to the space group $P2_12_12$, with cell dimensions $a = 88.33$, $b = 144.45$, and $c = 83.37$ Å. The Matthews coefficient was calculated to be 2.67 Da/Å^3, assuming two molecules per asymmetric unit. A self-rotation function calculation with MolRep confirmed the presence of a noncrystallographic two-fold axis relating the two molecules in the asymmetric unit (*11*, *12*). The cell parameters for crystals of mutant and wild-type LC are similar.

Since the protein contains one zinc ion per molecule, single-wavelength anomalous dispersion (SAD) data were collected from the crystal of wild-type LC at the zinc absorption edge ($\lambda = 1.2837$ Å) corresponding to the peak obtained at the NSLS beamline X12C with a Brandeis CCD-based B4 detector. The crystal was briefly transferred to the mother liquor containing 15−20% glycerol and was mounted on a nylon loop and flash frozen immediately by plunging into liquid nitrogen. Data covering a total of 360° rotation in ϕ were collected, for an oscillation range of 1° per frame, using the "inverse geometry" method. Crystals diffracted to better than 2.1 Å resolution. Data from mutant crystals were collected at $\lambda = 1$ Å, and the diffraction limit was 1.9 Å. Data were processed with DENZO and scaled and merged with SCALEPACK (*13*). Details of data collection statistics are given in Table 1.

Structure Determination. Initial attempts to determine the structure by the molecular replacement method using BoNT/A or BoNT/B LC as the search model failed. However, the method was not tried extensively. The data collected at the zinc absorption edge were used to solve the structure by the SAD method. The positions of the two zinc atoms were determined from the anomalous difference Patterson maps (*14*). The data were phased using SHARP (*15*) and further improved by noncrystallographic symmetry averaging and solvent flattening using DM (*16*). ARP/wARP (*17*) was used to build the model. About 70% of the model was built automatically by the program, and the rest was built-in manually using "O". The model was refined using CNS (*18*), and the solvent molecules were added using CNS. Initial refinements were carried out using strict NCS restraint. In the final stages this was relaxed, and both monomers were refined as independent molecules. The final model is complete, except for residues 234−244 and the 10 C-terminal residues in both molecules because of weak electron density, indicating that the region may be disordered. The rmsd between the C-α atoms of the two monomers in the asymmetric unit is 0.53 Å, excluding 16 C-terminal residues present in the structure. The two molecules differ in the

Table 1: Crystal Data and Refinement Statistics

Cell Parameters	
wild-type LC	space group $P2_12_12$ $a = 88.33$, $b = 144.45$, and $c = 83.27$ Å
Glu212Gln-LC	space group $P2_12_12$ $a = 88.21$, $b = 144.30$, and $c = 82.59$ Å

Phasing Statistics (Wild-Type-LC)	
method	SAD
wavelength (Å)	1.2837
anomalous scatterer	zinc
resolution (Å)	2.16
no. of reflections	56 133
overall FOM	0.15
after solvent flattening	0.91

Refinement Statistics

	wild-type LC	Glu212Gln-LC
resolution range (Å)	2.16	1.9
no. of reflections	55 960	74 652
completeness (%)	97.4	89.2
R-factor	0.22	0.24
R-free	0.26	0.29
no. of protein atoms	6315	6562
no. of heterogen atoms	3	4
no. of water molecules	348	493
rms deviations		
bond lengths (Å)	0.006	0.006
bond angles (°)	1.31	1.26

conformation of these C-terminal residues. The final *R* and *R*-free values are 0.22 and 0.26, respectively. A difference Fourier map brought out a chlorine ion near Arg 401. The reliability of the model was checked with PROCHECK (*19*), which showed that 88% of the residues are in the most favored region of the Ramachandran plot.

The structure of the mutant Glu212Gln was determined by the molecular replacement method, and the model was adjusted against a composite omit map to remove the model bias. Initially, during the molecular replacement Glu212 was substituted with alanine and the active-site zinc was not included in the search model. Gln was fitted into the density during model adjustment, and there was clear electron density for zinc. The model was refined using CNS. The final *R* and *R*-free values are 0.24 and 0.29, respectively. Clear electron density for residues 234−244 of the loop region missing in the wild-type protein structure was present in the mutant structure. The refinement statistics are presented in Table 1.

RESULTS AND DISCUSSIONS

Enzymatic Activity of BoNT/E-LC and Its Mutant Glu212Gln. The proteins were overexpressed in BL21 (DE3) cells, and use of the modified protocol as described in the methods section led to a very high recovery of protein. The protein was soluble and maintained its full length only when preserved at <-20 °C. The protein has been found to be temperature sensitive, and the preservation of protein at temperatures 4 °C or above led to the cleavage of ~2 kDa from the N-terminal of the protein.

The 49.7-kDa SNAP-25 tagged with GST (GST-SNAP-25) was used to assay the enzymatic activity of the BoNT/E-LC and its mutant (Glu212Gln). The GST tag was not removed from SNAP-25 since its presence in the fusion protein GST-SNAP-25 does not interfere with the catalytic activity of botulinum neurotoxins (*11*, *20*, *21*).

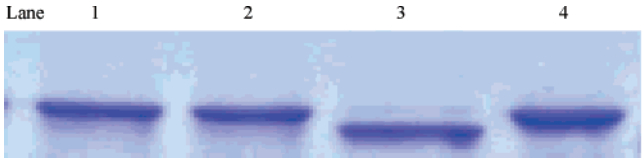

FIGURE 1: Analysis of catalytic activity of Glu212Gln mutant vs wild-type enzyme on its substrate SNAP-25. The reaction samples were run on 4−20% Tris−glycine gel and then stained with Coomassie blue. Lane 1 and 2, 5 and 50 nM mutant with 5 μM SNAP-25; lane 3, 5 nM wild-type enzyme with 5 μM SNAP-25; lane 4, 5 μM SNAP-25 alone. Using higher concentrations of mutant did not result in substrate cleavage.

Incubation of GST-SNAP-25 with BoNT/E-LC resulted in cleavage of peptide bond 180−181 of SNAP-25 and produced two fragments of sizes ~46.8 and ~2.9 kDa. The percentage cleavage of the substrate by enzyme at different time intervals showed that 5 nM LC was able to completely cleave 5 μM SNAP-25 in 15 min of incubation at 37 °C, suggesting that the protein is highly catalytic.

However, the Glu212Gln-LC mutant did not show any detectable activity. Increasing the mutant LC concentration did not lead to any cleavage product visible in the gel (Figure 1). The loss of activity may be because of loss of zinc, since the apo protein devoid of zinc is inactive. Spectroscopic analysis of zinc content was not done in this study and was not necessary, since during X-ray data collection the crystal was scanned at the absorption edge of zinc and a good signal for zinc was obtained, confirming the presence of zinc. Also, the structure determination brought out electron density for zinc.

The loss of catalytic activity could be either due to the enzyme not binding to the substrate or due to the loss of hydrolysis of the peptide. A control experiment was performed to identify the exact reason. The mutant and the substrate were mixed in a 1:1 ratio in the same buffer used for the wild-type enzyme and incubated for 30 min. The wild-type protein was then added in a 1:500 (enzyme to substrate) ratio and incubated at 37 °C for 30 min. An SDS gel was run to compare the results. There was no detectable cleavage of the substrate by the wild-type enzyme when the substrate was premixed with the mutant, indicating that the mutant effectively binds to the substrate and the wild-type enzyme has to compete for the binding site. As another control, the same experiment was repeated with the substrate premixed with an unrelated protein BSA, and the cleaved product was visible in the gel, showing that the binding of mutant to the substrate is specific. The control experiment was also repeated with another unrelated protein lysozyme, giving the same result. These two experiments confirmed that the mutant binds and positions itself for the catalytic activity but the peptide hydrolysis is blocked. In another experiment, we have also found that the Glu212Ala mutant of BoNT/E-LC forms a stable complex with GST-SNAP-25 at 4 °C (unpublished results).

Description of Structures of BoNT/E-LC. (a) Wild-Type BoNT/E-LC. This is the first time, at least to our knowledge, that the crystal structure of a molecule of this size (421 amino acids) has been determined using the anomalous signal from a single zinc atom, even though the contribution to the intensity from the anomalous signal from zinc ($f' = -8.1$

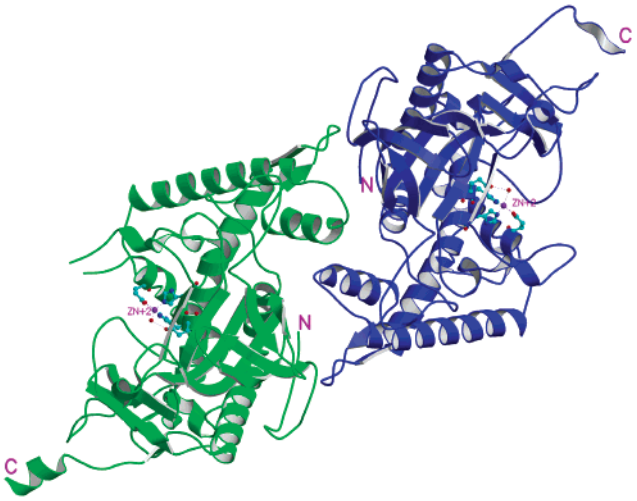

FIGURE 2: Ribbons representation of the dimer of BoNT/E-LC. Thesis composed of one monomer of wild-type (green) and one monomer of mutant (blue). The active-site zinc and coordinating residues are shown in the ball-and-stick model. The dimer is formed by a noncrystallographic two-fold axis passing through the midpoint normal to the plane of the figure. The C-terminal helix in the second monomer is not well ordered.

and f''= 3.89) is calculated to be less than 2% at 2.0 Å resolution. Since no other information was used in the structure determination, this must be considered a de novo structure determination without any model bias. Even though crystal structures of BoNT/A-LC and BoNT/B-LC have been determined, both of them are truncated version of the LC, unlike BoNT/E-LC. However, 10 C-terminal residues were not located in the electron density map. But a mass spectroscopic analysis of the protein gave the mass corresponding to full-length LC. Moreover, a few more residues (though disordered) were seen in the mutant structure, confirming that the missing residues are not due to any proteolysis. The BoNT/E-LC forms a dimer in the crystal and presumably a dimer in solution state also (Figure 2). Interestingly, unlike BoNT/A-LC, where the dimer is formed with the active site covered by the dimeric interface (unpublished work), here the active sites are not in the dimeric interface and are exposed to the solvent region. The advantage of this crystal structure is that it can be used for inhibitor studies by soaking native crystals in an inhibitor containing the mother liquor. The dimer is formed by a noncrystallographic two-fold symmetry. The buried surface area at the dimeric interface is 2340 Å^2.

The conformation of BoNT/E-LC is similar to those of BoNT/A-LC and BoNT/B-LC. One major difference may be at the C-terminus (Figure 3a). In BoNT/E-LC, which is a full-length LC, the C-terminal region takes a helical conformation. This region is just before the interchain disulfide bond. In BoNT/A and BoNT/B holotoxin structures, these are β strands. If BoNT/E holotoxin has a similar conformation, the change in conformation may be due to the separation of LC from HC or an artifact of recombinant protein. Since both BoNT/A and /B LCs are truncated LCs, their conformation in this region could not be directly compared with that of BoNT/E-LC.

The active site is similar to other botulinum neurotoxins. The active-site zinc is coordinated by His 211 NE2, His 215 NE2, Glu 250 OE1, Glu 250 OE2, and a nucleophilic water molecule (Figure 4a). The coordinating distances are given in Table 2. The nucleophilic water makes a hydrogen bond of 2.86 Å with Glu 212 OE2. This interaction seems to be important for the activation of the nucleophilic water.

About 45 residues are observed within a sphere of radius 10.0 Å centered on the zinc atom. Comparison of the residues in similar spheres in BoNT/B-LC and BoNT/A-LC brings out some interesting features. A few interactions are common to all of them. Glu 335 makes hydrogen-bonding contacts with Arg 347 and His 211, while Glu 249 interacts with His 215 and His 218, stabilizing the structure and the electrostatic forces (Figure 4). These interactions stabilize the side-chain conformations of His 211 and His 215, allowing them to be properly oriented for zinc coordination. Since these residues are conserved in all *Clostridium* neurotoxins (Figure 5), their role may be the same in all of them. Arg 347 and Tyr 350, which are in the active-site region, are similarly placed in BoNT/B-LC and BoNT/E-LC with respect to the nucleophilic

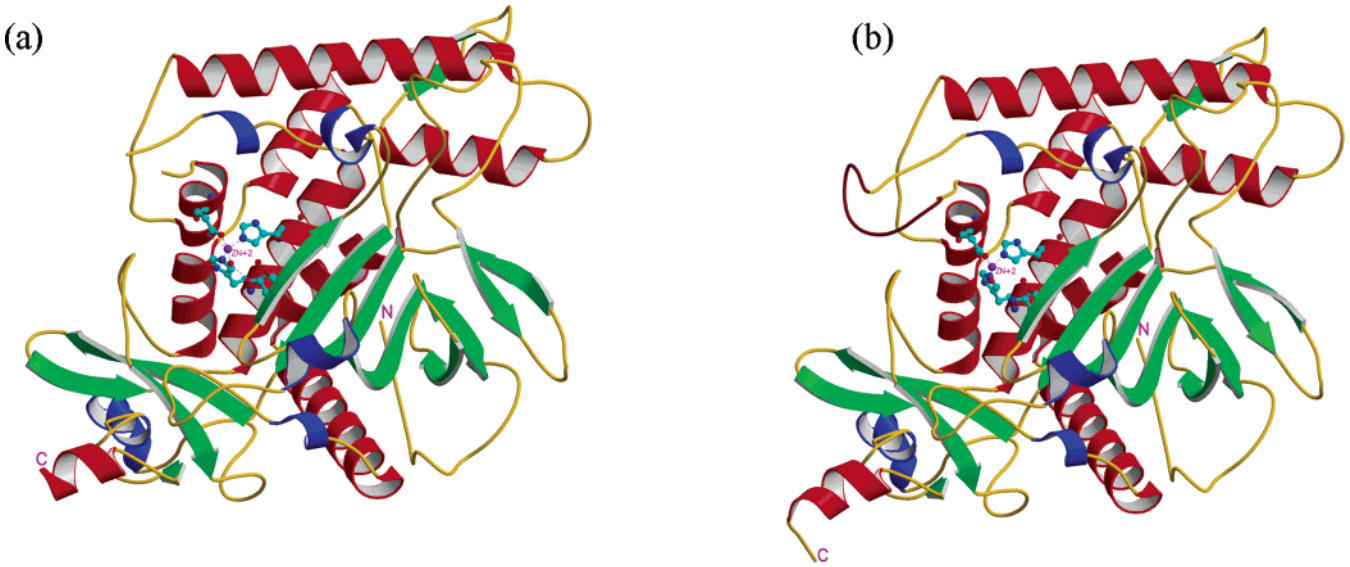

FIGURE 3: Ribbons representation of one monomer of (a) BoNT/E-LC and (b) the mutant Glu212Gln, with zinc and the coordinating residues shown as a ball-and-stick model. The loop region 234−244, which is ordered in the mutant, is shown in brown, while it is missing in the wild type. A few more C-terminal residues were modeled in the mutant than in the wild type.

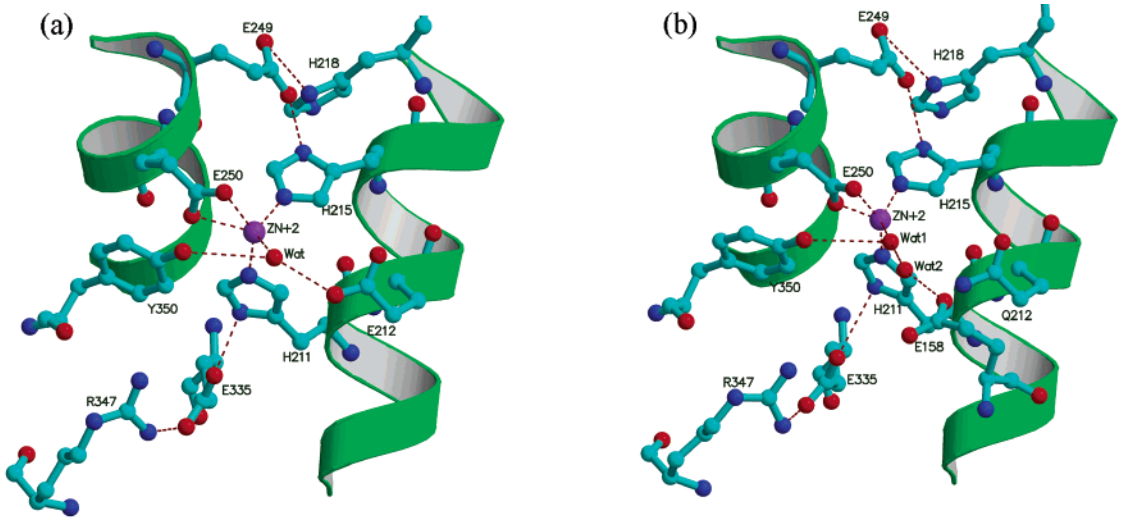

FIGURE 4: Interactions and hydrogen-bonding scheme of relevant residues which are conserved in BoNT/A, /B, and /E LCs. Hydrogen bonds are shown as dashed lines in red. (a) BoNT/E-LC and (b) the mutant Glu212Gln. The water molecule labeled "Wat1" in (b) corresponds to the nucleophilic water but has no hydrogen-bonding interaction with Gln 212.

Table 2. Relevant Interactions (Å) in BoNT/A, /B, and /E and the Mutant Glu212Gln[a]

	BoNT/ E-LC	mutant E212Q	BoNT/ A-LC	BoNT/ B-LC
Zn−H211 NE1	2.18	2.05	2.23	2.11
Zn−H215 NE2	2.16	2.20	2.22	2.15
Zn−E250 OE1	2.22	2.03	2.35	2.60
Zn−E250 OE2	2.46	2.83	2.64	2.20
Zn−Nu. water	2.17	2.79	2.75*	2.08
Nu. water−E212OE1	4.03	4.49	3.42*	3.54
Nu. water−E212OE2	2.86	3.46[b]	2.74*	2.80
Nu. water−Y350-OH	3.58	3.37	10.20*	4.62
Nu. water−E250 OE1	3.15	3.88	4.87*	3.11
Nu. water−R347NH2	7.06	6.92	7.40*	7.46
E335OE1−H211ND1	2.61	2.56	2.66	2.71
E335OE2−R347NH1	2.99	3.19	5.08	3.04
E249OE1−H215ND1	2.76	2.76	3.33	3.03
E249OE1−H218ND1	2.73	2.86	2.92	2.73
Y350-OH−Zn	3.94	3.95	8.10	4.3
Y350-OH−E250OE1	3.15	3.50	5.78	3.69
Y350-OH−E250OE2	3.43	3.30	6.53	3.70
R347NH−Zn	7.08	7.18	7.30	6.5

[a] The numbering scheme in the first column corresponds to BoNT/E. The numbers might vary for other LCs but the amino acids are conserved. In BoNT/A-LC the nucleophilic water (Nu. water) is displaced by Tyr 249 O and marked by an asterisk (*). [b] NE2.

water and the zinc. However, in BoNT/A-LC the corresponding tyrosine residue is farther away from the nucleophilic water. This discrepancy may be due to the autocatalytic nature of BoNT/A-LC, since the peptide bond between Tyr 249 and Tyr 250 is cleaved, as seen in the crystal structure, and positioning of Tyr 249 near the active site might have caused steric problem for Tyr 350 (*22*, *23*). Accordingly, the conserved residues Arg 347 and Tyr 350 may also play similar roles in all serotypes. Mutating residues corresponding to Arg 347 and Tyr 350 reduced the catalytic activity in BoNT/A (*24*) but did not completely abolish the activity. In the same study, it was shown that mutating residue corresponding to Glu 335 (Glu 350 in BoNT/A) drastically reduced the proteolytic activity (*24*). Since the interactions are identical in all serotypes, the effect of mutating these residues in BoNT/E will be the same. We have also shown that Glu 212 Gln completely abolishes the activity, similar to what was observed in BoNT/A (*25*). However, other residues in this sphere and beyond are not conserved and may be responsible for the specificity and selectivity of the toxins. In addition to coming close to zinc and the nucleophilic water, Tyr 350 is only 3.15 Å away from Glu 250 OE1. The interactions between the side-chain carboxylate of Glu 250 and the phenyl ring atoms of Tyr 350 could be characterized as aromatic−anion interactions (*26*). These interactions and the interaction of the hydroxyl group with the nucleophilic water might be stabilizing the side-chain orientation of Glu 250 and the transition state. Loss of this interaction may be one reason why the activity is decreased when Tyr 350 is mutated.

(b) Mutant BoNT/E-LC (Glu212Gln). The crystal structure of the mutant is very similar to the wild-type structure (Figure 3b). Overall, there is no conformational change, and the secondary structural elements are the same. The electron density for 234−244, which was weak in the wild-type structure, was continuous and well defined in the mutant structure. The only difference between the wild type and the mutant is the substitution of Glu with Gln at 212. Though the side-chain orientations of Gln and Glu are very similar, there is no hydrogen-bonding interaction with Gln 212 OE1 or NE2 (distances >3.5 Å), thereby increasing the distance between zinc and the nucleophilic water to 2.8 Å from 2.2 Å in the wild type (Figure 4). This water molecule (which is not a nucleophilic water anymore) is stabilized by a network of water molecules leading up to Glu 158. The charge distribution at the active sites of both wild-type and mutant structures is presented in Figure 6. Since there is no change in the structural features, the inductive effects exerted by the carboxylate side chain of Glu 212 in the wild-type L chain on neighboring groups must be responsible for the pronounced negative surface charge in the periphery of the active site. In other words, the neutralizing effect of the amide group of Gln 212 may be responsible for the decreased negative surface charge. In any case, it is evident that the change in the charge on Glu/Gln disturbs the electrostatic properties of the molecule at the active site, inactivating the toxin.

```
BoNT/B   RRVPLEEFNTNIASVTVNKLISNPGEVERKKGIFANLIIFGPGPVLNENETIDIGIQN-H 179
BoNT/E   DNTPDNQFHIGDASAVEIKFSNGSQDI-----LLPNVIIMGAEPDLFETNSSNISLRNNY 170
BoNT/A   STIDTELKVIDTNCINVIQPDGSYRSE------ELNLVIIGPSADIIQFECKSFGHEVLN 173

BoNT/B   FASREGFGGIMQMKFCPEYVSVFNNVQENKGASIFNRRGYFSDPALILMHELIHVLHGLY 239
BoNT/E   MPSNHGFGSIAIVTFSPEYSFRFNDNSMN---------EFIQDPALTLMHELIHSLHGLY 221
BoNT/A   LTRN-GYGSTQYIRFSPDFTFGFEESLEVDTNPLLGAGKFATDPAVTLAHELIHAGHRLY 232

BoNT/B   GIK-VDDLPIVPNEKKFFMQSTDA-IQAEELYTFGGQDPSIITPSTDKSIYDKVLQNFRG 297
BoNT/E   GAKGITTKYTITQKQNPLITNIRG-TNIEEFLTFGGTDLNIITSAQSNDIYTNLLADYKK 280
BoNT/A   GIAINPNR-VFKVNTNAYYEMSGLEVSFEELRTFGGHDAKFIDSLQENEFRLYYYNKFKD 291

BoNT/B   IVDRLNKVLVCISD-PNININIYKNKFKDKYKFVEDSEGKYSIDVESFDKLYKSLMFGFT 356
BoNT/E   IASKLSKVQVSNP-----LLNPYKDVFEAKYGLDKDASGIYSVNINKFNDIFK-KLYSFT 334
BoNT/A   IASTLNKAKSIVGT--TASLQYMKNVFKEKYLLSEDTSGKFSVDKLKFDKLYKMLTEIYT 349

BoNT/B   ETNIAENYKIKTRASYFSDSLPPVKIKNLLDNEIYTIEEGFNISDKDMEKEYRGQNKAIN 416
BoNT/E   EFDLATKFQVKCRQTYIG-QYKYFKLSNLLNDSIYNISEGYNINN--LKVNFRGQNANLN 391
BoNT/A   EDNFVKFFKVLNRKTYLNFDKAVFKIN-IVPKVNYTIYDGFNLRNTNLAANFNGQNTEIN 408
```

FIGURE 5: Sequence comparison of residues of BoNT/A, /B, and /E (only part of the sequence of LC is shown). The conserved residues are shaded in gray, and residues coordinated to zinc are in boxes. Arg 347 and Tyr 350, presumably involved in transition-state stabilization, are in bold. The underlined residues fall within a sphere of 10-Å radius centered on the active-site zinc. Other residues involved in the catalytic pathway and shown in Figure 7 are shown in white against a black background.

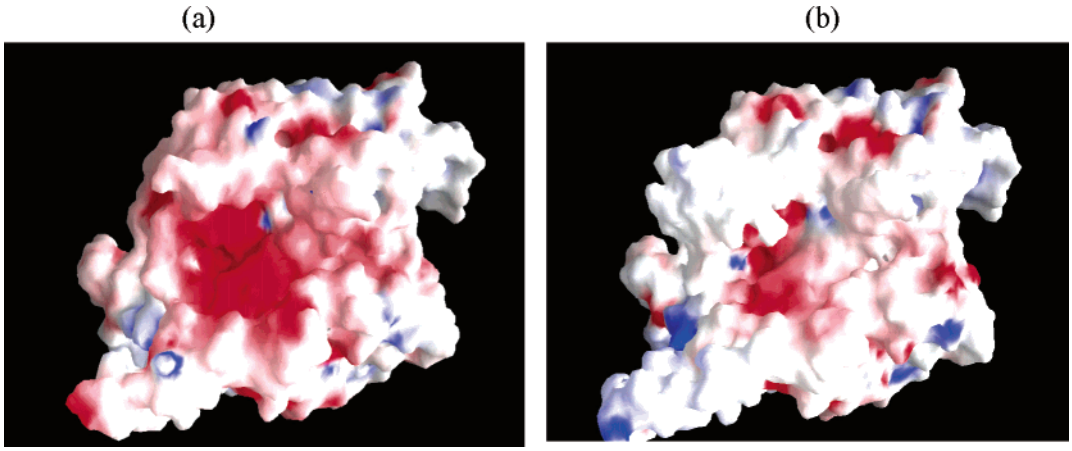

FIGURE 6: Electrostatic potential surfaces of (a) BoNT/E-LC and (b) the mutant Glu212Gln. The positive and negative electrostatic potentials are represented in blue and red. The active site in the wild type is highly negative compared to that in the mutant. In the mutant (b), the active site is partly covered by the loop 234−244 (top left of the figure), which is missing in the wild type.

Since it has been shown in BoNT/A-LC that mutating residues corresponding to Arg 347 and Tyr 350 only reduces but does not completely abrogate the activity, they may not play a major role in the catalytic activity but play a role in stabilizing the transition state. Also, the reduction of the K_{cat} value is much more when Arg 347 is mutated than for Tyr 350 mutation, implying that Tyr 350 plays a less critical role for transition-state stabilization than Arg 347. In any case, they may not act as proton donor for the leaving amide group, in which case the activity would have been lost completely (*24*). However, as we have shown here for BoNT/E-LC, the activity is completely lost when Glu 212 is changed to Gln 212, as in the case of BoNT/A-LC (*25*). These observations, taken together with the movement of nucleophilic water, gives a model for the catalytic activity and the importance of the nucleophilic water and Glu 212. It is evident that Glu 212 helps the leaving group by transferring/shuttling two protons from the nucleophilic water. Our model here is consistent with what we had proposed for BoNT/B (Figure 7) (*27*). The carbonyl oxygen of the scissile bond is polarized by the nucleophilic water, which moves closer to Glu 212 but still maintains its interaction with zinc. The transition tetrahedral state of the carbonyl carbon is stabilized by Arg 347 and Tyr 350. Protons are shuttled to the leaving group in two stages. This scenario is slightly at variance with that proposed for TeNT, where the corresponding tyrosine is suggested to be the proton donor (*28*). It may be that the scheme is somewhat different for TeNT from BoNTs.

Three loops were identified in BoNT/B-LC to have changed conformation when the LC separates from the heavy chain (*8*). Though we see possible changes in conformations of these loops, the extent of the changes seems to be less. When BoNT/A, /B, and /E LCs are compared, loop 50 in BoNT/A-LC seems to take a different conformation. However, this region is not well defined in the electron density map. A direct comparison of loop 250 could not be made since the loop is cleaved in the BoNT/A-LC structure (Figure 8).

This study supports the fact that substitution of the Glu 212 by Gln 212 in the active site leads to the loss of the enzymatic activity of the protein. Structural data suggest that the loss in activity of the protein is not the result of folding

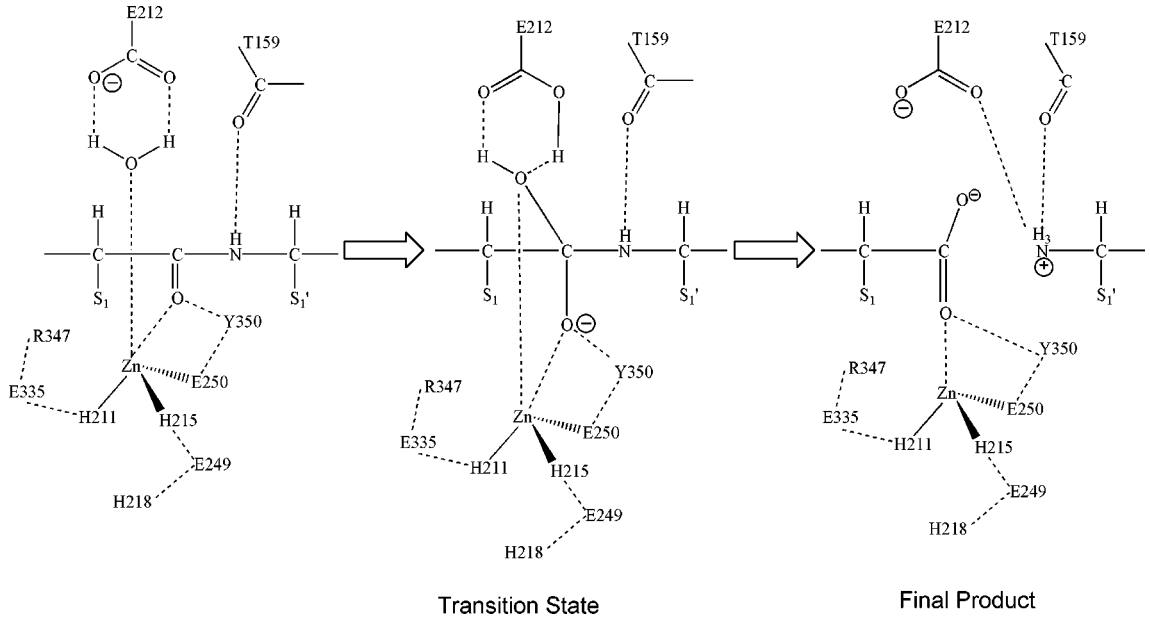

FIGURE 7: Catalytic pathway model for BoNT/E-LC based on our present and previous results. Glu 212 serves as a general base for the catalytic activity and shuttles two protons to the leaving group. His 218, Glu 249, Glu 335, Arg 347, and Tyr 350, stabilizing the orientation of the histidines or the transition state, are also shown, along with Thr 159. While experimental evidence for the role of Glu 249 and His 218 is not yet available, Thr 159 is included here in analogy with our work on BoNT/B (*27*). S1 and S1′ are Arg 180 and Ile 181 of SNAP-25. Hydrogen-bonding interactions and anion−aromatic interactions (Tyr 350−Glu 250) are shown by dashed lines.

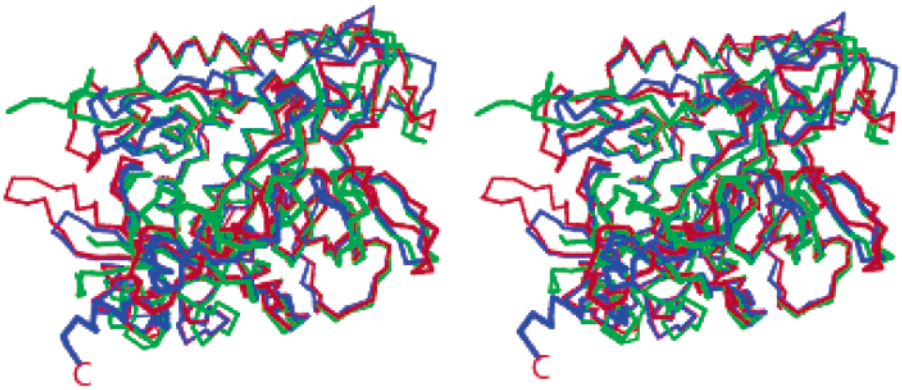

FIGURE 8: Stereographic view of a comparison of C-α traces of BoNT/A (green), /B (red), and /E (blue). Except for the loop regions, the conformations are similar.

variation but rather is due to the close involvement of the negative charge of the carboxylate group which directly participates in the hydrolysis of the substrate. The distance and the topographical positioning of the carboxylate group play essential roles in the substrate hydrolysis.

CONCLUSIONS

The present study reveals the role of the nucleophilic water and the charge on Glu212 on the catalytic activity. It also provides a method for developing a novel genetically modified protein vaccine. It suggests that a sensitive inhibitor could be developed if Glu212 is blocked or covalently modified and may well become a common drug for all serotypes. Since the conformation of the mutant is almost identical to that of the wild-type protein and it effectively binds to the substrate, the mutant offers itself as a candidate for studying the enzyme−substrate complex without the substrate being cleaved.

ACKNOWLEDGMENT

We thank Dr. A. Saxena for providing beam time on X12C of the National Synchrotron Light Source, Brookhaven National Laboratory, J. Romeo for technical assistance, and Drs. J. J. Dunn and C. B. Millard for helpful discussions. T.B. was supported by a grant from the Deutsche Forschungsgemeinschaft. A small gift from Allergan, USA, is gratefully acknowledged.

REFERENCES

1. Schiavo, G., Matteoli, M., and Montecucco, C. (2000) Neurotoxins affecting neuroexocytosis, *Physiol. Rev. 80*, 717−766.
2. Schiavo, G., Santucci, A., Dasgupta, B. R., Metha, P. P., Jontes, J., Benfenati, F., Wilson, M. C., and Montecucco, C. (1993) Botulinum neurotoxins serotypes A and E cleave SNAP-25 at distinct COOH-terminal peptide bonds, *FEBS Lett. 335*, 99−103.
3. Binz, T., Blasi, J., Yamasaki, S., Baumeister, A., Link, E., Sudhof, T. C., Jahn, R., and Niemann, H. (1994) Proteolysis of SNAP-25 by Types E and A botulinum neurotoxins, *J. Biol. Chem. 269*, 1617−1620.

4. Vaidyanathan, V. V., Yoshino, K., Jahnz, M., Dorries, C., Bade, S., Nauenburg, S., Niemann, H., and Binz, T. (1999) Proteolysis of SNAP-25 isoforms by botulinum neurotoxin types A, C, and E: Domains and amino acid residues controlling the formation of enzyme−substrate complexes and cleavage, *J. Neurochem. 72*, 327−337.
5. Montecucco, C., and Schiavo, G. (1995) Structure and function of tetanus and botulinum neurotoxins, *Q. Rev. Biophys. 28*, 423−472.
6. Lacy, D. B., Tepp, W., Cohen, A. C., DasGupta, B. R., and Stevens, R. C. (1998) Crystal structure of botulinum neurotoxin type A and implications for toxicity, *Nat. Struct. Biol. 5*, 898−902.
7. Swaminathan, S., and Eswaramoorthy, S. (2000) Structural analysis of the catalytic and binding sites of *Clostridium botulinum* neurotoxin B, *Nat. Struct. Biol. 7*, 693−699.
8. Hanson, M. A., and Stevens, R. C. (2000) Cocrystal structure of synaptobrevin-ll bound to botulinum neurotoxin type B at 2.0 A resolution, *Nat. Struct. Biol. 7*, 687−692.
9. Umland, T. C., Wingert, L. M., Swaminathan, S., Furey, W. F., Schmidt, J. J., and Sax, M. (1997) Structure of the receptor binding fragment H_c of tetanus neurotoxin, *Nat. Struct. Biol. 4*, 788−792.
10. Emsley, P., Fotinou, C., Black, I., Fairweather, N. F., Charles, I. G., Watts, C., Hewitt, E., and Isaacs, N. W. (2000) The structures of the H(C) fragment of tetanus toxin with carbohydrate subunit complexes provide insight into ganglioside binding, *J. Biol. Chem. 275*, 8889−8894.
11. Agarwal, R., Eswaramoorthy, S., Kumaran, D., Dunn, J. J., and Swaminathan, S. (2004) Cloning, high level expression, purification and crystallization of the full length Clostridium botulinum neurotoxin type E light chain, *Protein Expr. Purif. 34*, 95−102.
12. Vagin, A., and Teplyakov, A. (2000) An approach to multi-copy search in molecular replacement, *Acta Crystallogr. D56*, 1622−1624.
13. Otwinowski, Z., and Minor, W. (1997) Processing of X-ray diffraction data collected in oscillation mode, *Methods Enzymol. 276*, 307−326.
14. Furey, W., and Swaminathan, S. (1997) PHASES-95: A program package for the processing and analysis of diffraction data from macromolecules., *Methods Enzymol. 276*, 590−620.
15. De La Fortelle, E., and Bricogne, G. (1997) Maximum-likelihood heavy atom parameter refinement in the MIR and MAD methods, *Methods Enzymol. 276*, 472−493.
16. Cowtan, K. (1994) *Joint CCP4 ESF-EACBM Newsl. Protein Crystallogr. 31*, 34−38.
17. Perrakis, A., Morris, R., and Lamzin, V. S. (1999) Automated protein model building combined with iterative structure refinement, *Nat. Struct. Biol. 6*, 458−463.
18. Brunger, A. T., Adams, P. D., Clore, G. M., Delano, W. L., Gros, P., Grosse-Kunstleve, R. W., Jiang, J. S., Kuszwewski, J., Nilges, M., Pannu, N. S., Read, R. J., Rice, L. M., Somonsom, T., and Warren, G. L. (1998) Crystallography & NMR system: a new software suite for macromolecular structure determination, *Acta Crystallogr. D54*, 905−921.
19. Laskowski, R. A., MacArthur, M. W., Moss, D. S., and Thornton, J. M. (1993) PROCHECK: a program to check the stereochemical quality for assessing the accuracy of protein structures, *J. Appl. Crystallogr. 26*, 283−291.
20. Washbourne, P., Pellizzari, R., Baldini, G., Wilson, M. C., and Montecucco, C. (1997) Botulinum neurotoxin A and E require the SNARE motif in SNAP-25 for proteolysis, *FEBS Lett. 418*, 1−5.
21. Rigoni, M., Caccin, P., Johnson, E. A., Montecucco, C., and Rossetto, O. (2001) Site-directed mutagenesis identifies active-site residues of the light chain of botulinum neurotoxin type A, *Biochem. Biophys. Res. Commun. 288*, 1231−1237.
22. Ahmed, S. A., and Smith, L. A. (2000) Light chain of botulinum A neurotoxin expressed as an inclusion body from a synthetic gene is catalytically and functionally active, *J. Protein Chem. 19*, 475−487.
23. DasGupta, B. R., and Foley, J. (1989) C. Botulinum neurotoxin types A and E: isolated light chain breaks down into two fragments. Comparison of their amino acid sequences with tetanus neurotoxin, *Biochemie 71*, 1193−1200.
24. Binz, T., Bade, S., Rummel, A., Kollewe, A., and Alves, J. (2002) Arg^{362} and Tyr^{365} of the botulinum neurotoxin type A light chain are involved in transition state stabilization, *Biochemistry 41*, 1717−1723.
25. Li, L., Binz, T., Niemann, H., and Singh, B. R. (2000) Probing the mechanistic role of glutamate residues in the zinc-binding motif of type A botulinum neurotoxin light chain, *Biochemistry 39*, 2399−2405.
26. Jalbout, A. F., and Adamowicz, L. (2002) Anion-aromatic molecule complex. *Ab initio* study of the benzene.O_2 anion, *J. Chem. Phys. 116*, 9672−9676.
27. Swaminathan, S., Eswaramoorthy, S., and Kumaran, D. (2004) Structure and enzymatic activity of botulinum neurotoxins, *Mov. Disord. 19* (Suppl. 8), S17−S22.
28. Rossetto, O., Caccin, P., Rigoni, M., Tonello, F., Bortoletto, N., Stevens, R. C., and Montecucco., C. (2001) Active-site mutagenesis of tetanus neurotoxin implicates TYR-375 and GLU-271 in metalloproteolytic activity, *Toxicon 39*, 1151−1159.

BI036278W